

# Abundant Production of Reactive Water Radical Cations under Ambient Conditions

Meng Wang<sup>1</sup>', Xiao-Fei Gao<sup>1</sup>', Rui Su<sup>2</sup>, Peng He<sup>1</sup>, Yuan-Yuan Cheng<sup>1</sup>, Ke Li<sup>1</sup>, Dongbo Mi<sup>1</sup>, Xiaoping Zhang<sup>1</sup>, Xinglei Zhang<sup>1</sup>, Huanwen Chen<sup>1</sup>\* & R. Graham Cooks<sup>3</sup>\*

<sup>1</sup>Jiangxi Key Laboratory for Mass Spectrometry and Instrumentation, East China University of Technology, Nanchang 330013, <sup>2</sup>State Key Laboratory of Inorganic Synthesis and Preparative Chemistry, College of Chemistry, Jilin University, Changchun 130012, <sup>3</sup>Department of Chemistry and Center for Analytical Instrumentation Development, Purdue University, West Lafayette, IN 47907

\*Corresponding authors: chw8868@gmail.com; cooks@purdue.edu; M. Wang and X.-F. Gao contributed equally to this work.

**Cite this:** *CCS Chem.* **2022**, 4, 1224–1231 **DOI:** 10.31635/ccschem.021.202101427

Water radical cations, the crucial intermediates in many aqueous reactions and biochemical processes, are difficult to investigate experimentally due to their short lifetime and low abundance. Herein, a homemade device based on energy-tunable discharge was employed to deposit suitable amounts of energy to atmospheric pressure pure water vapor for abundant production of water radical cations, stabilized as  $(H_2O)_n^{+\bullet}$  (n = 2-5) with a maximal abundance of  $\geq$ 8.3  $\times$  10<sup>6</sup> cps for  $(H_2O)_2^{+\bullet}$ , characterized by mass spectrometry (MS). The abundance of water radical cations was optimized by adjusting the experimental parameters such as the discharge voltage (2.5 kV), temperature of the MS inlet (140 °C), carrier gas flow (20 mL/min), and the distance between the discharge tip and MS inlet (12 mm). The ambient formation of water radical cations was further confirmed by the high reactivity of as-prepared water radical cations, which reacted with benzene, ethyl acetate, and dimethyl disulfide instantly, showing rich chemistry with ionic and radical characteristics. Moreover, the computations usingCCSD(T)//MP2 method and density functional theory confirmed that the O-O single-electron

bound dimer (B), as well as the hydronium hydroxyl radical complex (A), accounted for the unusual chemistry of the water radical cations, providing a facile approach to access the high reactivity of water radical cations under the ambient conditions.

Keywords: water, radical cation, mass spectrometry, O-O single-electron bound dimer of water radical cation, hydronium hydroxyl dimer of water radical cation

**DOI:** 10.31635/ccschem.021.202101427 **Corrected Citation:** *CCS Chem.* **2022**, 4, 1224–1231 **Previous Citation:** *CCS Chem.* **2021**, 3, 3559–3566 **Link to VoR:** https://doi.org/10.31635/ccschem.021.202101427



## Introduction

The study of systems comprising a small number of water molecules is a topic of immense interest. As well documented, functional biomolecules, such as DNA, 1,2 RNA, 3-5 and proteins, 6-10 are affected by the water molecules surrounding them. Besides neutral small clusters,7-11 the protonated forms, 12-14 starting with hydronium ion, have marked periodicity properties. Further, the bonding in hydrated electrons (solvated water radical anions) has been studied using detailed spectroscopy and computation.<sup>15-18</sup> By contrast, only a few reports on spectroscopy and computational studies 19-24 of the chemistry of the water radical cation and its solvated forms exist. This is probably due to the inconvenience of generating water radical cations with a small number of water solvation molecules responsible for this situation. To date, water radical cations have been created by exposing water vapor to vacuum-UV photoionization, 22,25,26 electron-impact ionization, 24,27,28 dinitrogen chemical ionization, 29-32 femtosecond multiphoton ionization,<sup>33</sup> photoionization in a supersonic jet expansion,<sup>34</sup> or soft X-ray radiation.<sup>35,36</sup> In general, methods of water radical cation formation reported previously have the following features: (1) water radical cation or the clusters  $(H_2O)_n^{+\bullet}$   $(n \le 10)$  were observed in extremely low yield;<sup>22,37</sup> (2) high vacuum  $(10^{-5} \sim 10^{-8} \; Torr)^{18,19,22,23,38}$  or low temperature (<20 K)  $^{24,36}$ were required to suppress their dissociation. However, when collisions with water vapor were allowed, the products were invariably the hydronium ion and its solvated clusters. These features have severely limited the access to the chemistry of water radical cations, particularly the  $(H_2O)_n^{+\bullet}$  (n = 1 ~ 3) species, believed to have fundamental significance in life science, physics, chemistry, biomedicine, and interstellar chemistry, since they are the key selfsolvated water radical cations.

Herein, we employed a homemade device based on energy-tunable discharge to generate water radical cations (n = 2-5) instead of high vacuum or low temperature with substantial amounts of mono-solvated water radical cation  $(H_2O)_2^{+\bullet}$  as the main product. The ionic products were conveniently characterized by tandem mass spectrometry (MS) experiments with additional information from isotopic labeling, computation, and high-resolution MS measurements. Furthermore, an ambient formation of water radical cations was experimentally confirmed by the high reactivity of the as-prepared water radical cations, which instantly reacted with ethyl acetate (EA), dimethyl disulfide, and benzene, showing the rich ionic and radical character of the O-O singleelectron bound dimer (B), as well as the hydronium hydroxyl radical complex (A). Therefore, our approach provides adequate water radical cations, which benefit advanced studies and applications of water clusters.

#### **Results and Discussion**

# Production and characterization of water radical cations

In our experiment, pure water evaporated freely, and the vapor was carried by an inert gas (e.g., N2, He, etc.) to intersect the ambient ionic plume generated by the energy-tunable corona discharge (Figure 1a). Under optimized conditions, the water radical cation signal  $H_2O^{+\bullet}$  (m/z 18) and its solvated counterpart  $(H_2O)_n^{+\bullet}$  (n = 2, 3; m/z 36, 54)were abundantly detected (Figure 1b) in the mass spectrum, with the dimer of m/z 36 being the base peak (>8.3  $\times$  10<sup>6</sup> cps). The assignments for the signals at m/z36 (Supporting Information Figure S1a) and m/z 54 (Supporting Information Figure S1b) were also validated by characteristic ionic fragments observed using tandem mass spectrometry<sup>37</sup> and high-resolution mass measurements (Supporting Information Figure S2). The mass spectral pattern presented in Figure 1b is an experimental data showing that the small water radical cation clusters  $(H_2O^{+\bullet}$  and  $(H_2O)_2^{+\bullet})$  were favorably formed rather than the large ones (( $H_2O)_n^{+\bullet}$ ,  $n \ge 3$ ). Extra reference experiments demonstrated that the production of water radical cations was not ratiocinated from the inert gases because no noted dependency of the signals (m/z 18, 36, and 54) on the gas (Ar, Ne, or He) used to transport the water vapor (Supporting Information Figure S3). The signal at m/z 55 was confirmed as  $(H_2O)_3H^+$  by collision-induced dissociation (CID) data (Supporting Information Figure S4) and high-resolution MS measurements (Supporting Information Figure S5). Additionally, the formation of water radical cations was verified using deuterated water to observe the water radical cations of  $(D_2O)_2^{+\bullet}$  (m/z 40) and  $(D_2O)_3^{+\bullet}$  (m/z 60) (inset of Figure 1b) in high abundance. Traces of  $D_2O^{+\bullet}$  ions (m/z 20) were also observable when the mass spectrum was expanded 100 times (inset of Figure 1b). The presence of adventitious water was also detectable from the isotopic composition of the monomer, dimer, and trimer clusters. These results indicated that the water radical cations were produced by energy-tunable discharge with relatively low energy.

Note that the hydronium ions were preferably produced, and the water radical cations were hardly detected if the corona discharge energy was not systematically optimized. However, abundant water radical cations were reproducibly obtained under the optimized experimental conditions. Figure 1c shows the MS signal intensities for m/z 36 and m/z 37 ions as a function of discharge voltage. With increased discharge voltage, the abundance of  $(H_2O)_2^{+\bullet}$  (m/z 36) increased slightly, while the abundance of  $(H_2O)_2^{+\bullet}$  (m/z 37) showed a steady increase. Thus, the intensity ratios between  $(H_2O)_2^{+\bullet}$  and  $(H_2O)_2^{+\bullet}$  decreased dramatically with increasing discharge voltage (Figure 1c), suggesting that the water radical cations were only



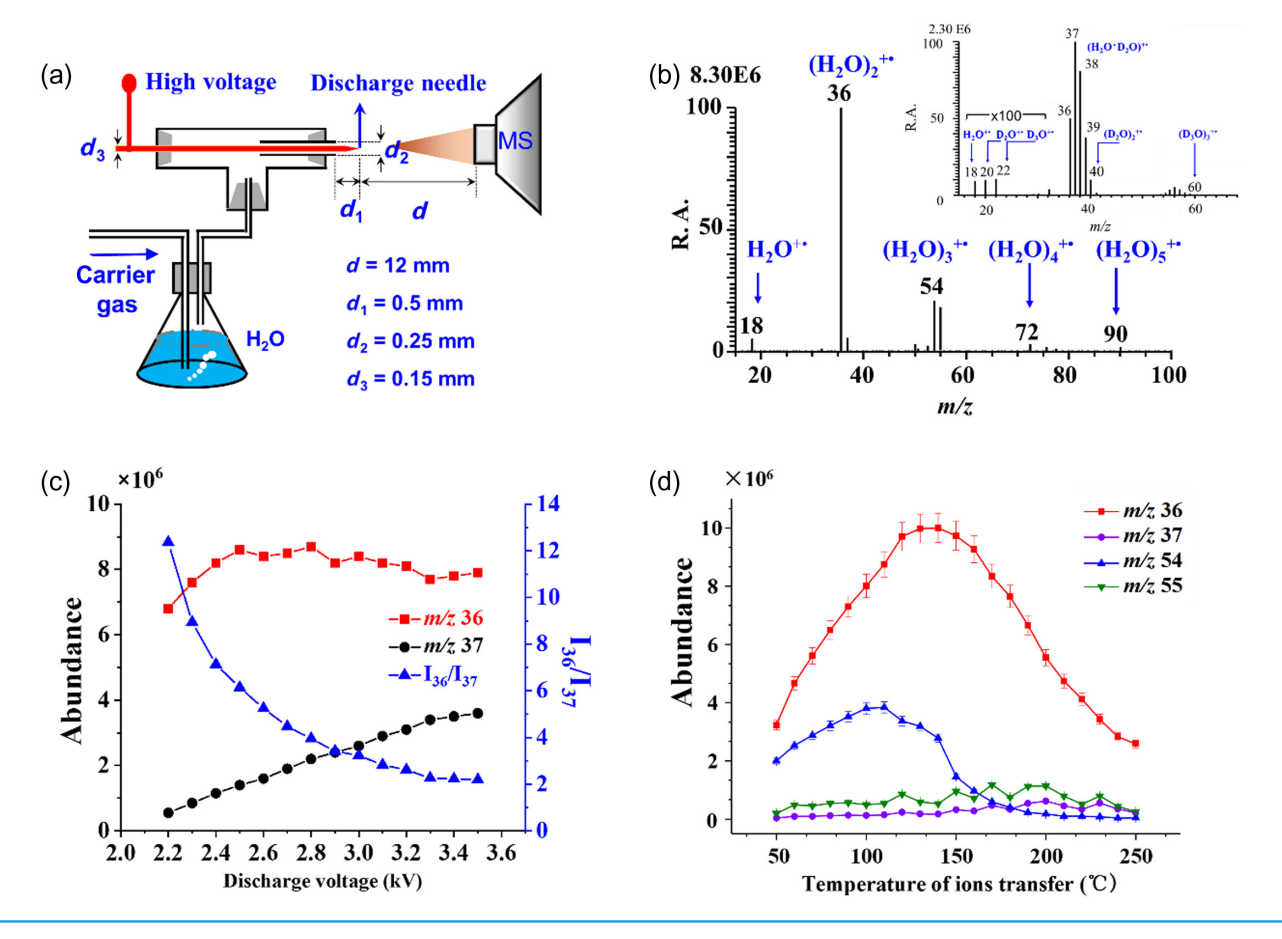


**Figure 1** | Ambient production of abundant water radical cations. (a) Schematic diagram of the energy-tunable discharge for generation of water radical cations. (b) Typical mass spectrum of water radical cations produced under optimized conditions using  $N_2$  as the carrier gas, inset: typical mass spectrum of deuterated water radical cations produced under the optimized conditions. (c) Peak intensities were detected at either m/z 36 or m/z 37 and their ratios ( $I_{36}/I_{37}$ ) as the function of discharge voltage. (d) MS signal intensities for ions m/z 36, m/z 37, m/z 54, and m/z 55 as the function of ions transfer temperature.

produced with a narrow range of suitable discharge voltage, by which a strong electric field was created to facilitate electron stripping from neutral water molecules. However, the radical cations were favorably dissociated into hydronium ions in the solvated form once excessive energy (i.e., high voltage  $\geq 2.5$  kV) was deposited to the water radical cations.

Similarly, other factors such as the capillary temperature, carrier gas flow rate, the distance between the discharge tip and the ion entrance, and so on, affect the total energy input onto the water radical cations. Figure 1d shows the MS signal intensities for m/z 36, m/z 37, m/z 54, and m/z 55 ions as a function of the capillary temperature used for ion transfer. As the temperature was increased, the abundance of  $(H_2O)_2^{+\bullet}$  (m/z 36) increased due to better dissolution/detection, and then decreased markedly at around 140 °C mainly because of the accelerated dissociation. Meanwhile, the ions of m/z 54 showed a similar temperature feature as the m/z 36 ions, but the breakdown temperature was about 100 °C, much lower

than that of the m/z 36 ions, probably because the three water molecules' cluster was broken more readily than the dimers under high temperature (≥100 °C). By contrast, the absolute abundance of  $(H_2O)_2H^+$  (m/z 37) and  $(H_2O)_3H^+$ (m/z 55) showed little temperature effects, probably due to enhanced stability of the hydronium ions than the radical cation clusters. These data suggested better performance of the m/z 36 ions if the capillary temperature should be maintained at about 140 °C. The overall effects of the carrier gas flow (Supporting Information Figure S6) and the distance between the discharge tip and the MS inlet (Supporting Information Figure S7) on the production of water radical cations are detailed in supporting information. Briefly, the gas flow rate did not provide differential tendency on the ions of either m/z 36 or m/z 37, probably because the effect was mainly caused by the collisions in the gaseous flow. The distance effect (Supporting Information Figure S7) was reciprocally similar to the contribution of the discharge voltage (Figure 1c), probably because the distance also correlated with energy.

**DOI:** 10.31635/ccschem.021.202101427 **Corrected Citation:** *CCS Chem.* **2022**, 4, 1224–1231 **Previous Citation:** *CCS Chem.* **2021**, 3, 3559–3566



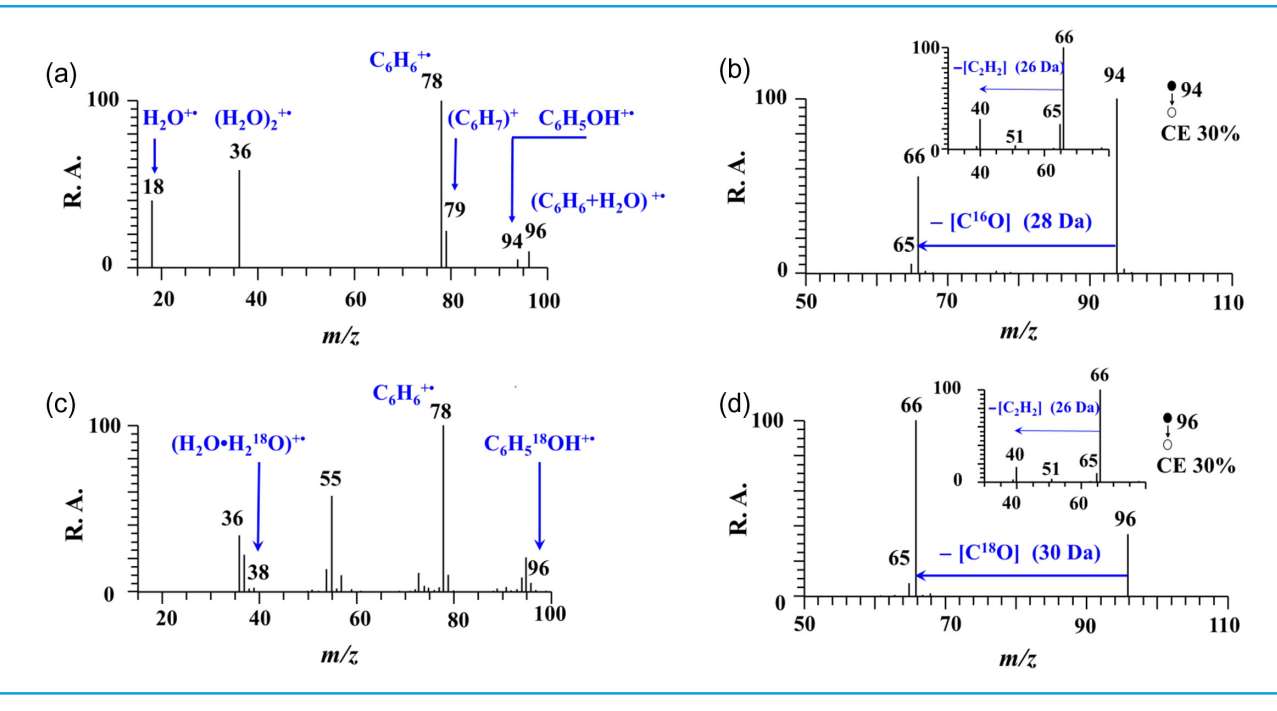


**Figure 2** | Mass spectrometric characterization of reaction between  $(H_2O)_2^{*\bullet}$  and benzene. (a) Typical mass spectrum collected with benzene present showing  $C_6H_5OH^{*\bullet}$  formation in the ion trap. (b) Collison-induced dissociation spectra of  $C_6H_5OH^{*\bullet}$ , m/z 94  $\rightarrow$  products, inset: m/z 94  $\rightarrow$  66  $\rightarrow$  products. (c) Typical mass spectrum with benzene and  $H_2^{18}O$  showing  $C_6H_5^{18}OH^{*\bullet}$  formation. (d) Collison-induced dissociation spectra of  $C_6H_5^{18}OH^{*\bullet}$ , m/z 96  $\rightarrow$  products, inset: m/z 96  $\rightarrow$  66  $\rightarrow$  products.

However, different discharge voltages with varying distances caused remarkable changes in the mass spectra (Supporting Information Figure S8). Taking both the abundance of  $(H_2O)_2^{+\bullet}$  and the abundance ratio of  $(H_2O)_2^{+\bullet}/(H_2O)_2^{+\bullet}$  into account, a discharge voltage of 2.5 kV, a distance of 12 mm, ion transfer temperature of 140 °C, and carrier gas flow of 20 mL/min represented the optimized conditions, providing a facile method for abundant production of water radical cations requiring neither high vacuum<sup>28-31</sup> nor low temperature.<sup>26</sup>

#### Chemical reactions of water radical cations

Theoretically, water radical cations should bestow unique chemistry through reaction with substances that might not react with water. Therefore, the possibility of water radical cations to react with chemical reagents and biofunctional groups were explored using benzene, EA, and dimethyl disulfides as the model compounds.  $(H_2O)_2^{+\bullet}$  was chosen as the main reactant as it has the highest abundance.

# Reactions of water radical cations and benzene

Benzene was introduced as vapor into the ion trap, where the  $(H_2O)_2^{+\bullet}$  ions (m/z 36) were mass-selectively isolated. Upon CID, the ions of the reactant, benzene

radical cations, and phenol radical cations (m/z 94) were detected in the spectrum (Figure 2a).  $H_2O^{+\bullet}$  (m/z 18) might be the by-product of self-dissociation of  $(H_2O)_2^{+\bullet}$ (m/z 36) in the ion trap reaction with benzene. The ions of m/z 94 produced characteristic fragments of m/z 66 and m/z 65 (Figure 2b) by the loss of neutral CO (28 Da) and [HCO] (29 Da), respectively. Furthermore, fragments of m/z 65 (tentatively the cyclopentadiene ion), m/z 51 (cyclobutadiene ion), m/z 40 (cyclopropene radical cation) were obtained by CID of ions of m/z 66 (inset of Figure 2b). The characteristic m/z 66 fragment of the phenol radical cation,  $C_6H_5OH^{+\bullet}$  (m/z 94), <sup>39,40</sup> produced an ion of m/z 40 (cyclopropene radical cation) through the elimination of acetylene (26 Da). These results strongly suggested that the ion of m/z 94 (the exact value at m/z94.0414) was the phenol radical cation C<sub>6</sub>H<sub>5</sub>OH<sup>+•</sup>, validated by the exact m/z matching experiments with high mass accuracy (1.0 ppm) (Supporting Information Figure S9a). The observation of phenol radical cation (m/z 94)indicated that  $(H_2O)_2^{+\bullet}$  showed characteristics of an OH radical. Thus, the phenol radical cation was produced, as presented in eq 1 below:

$$C_6H_6+(H_2O)_2^{+\bullet}\to C_6H_5OH^{+\bullet}+H_2O+H_2$$
 (1)

in which hydrogen gas was also detected and showed proportional respondence on the reactants and ion current (Supporting Information Figure S10). Furthermore,

**DOI:** 10.31635/ccschem.021.202101427 **Corrected Citation:** *CCS Chem.* **2022**, 4, 1224–1231

Previous Citation: CCS Chem. **2021**, 3, 3559–3566 Link to VoR: https://doi.org/10.31635/ccschem.021.202101427



the phenol cations were solflanded for characterization by infrared absorption (Supporting Information Figure S11) and liquid chromatography (Supporting Information Figure S12), which validated the production of phenol and hydrogen through eq 1.

When the reactant was isotope-labeled as H<sub>2</sub><sup>18</sup>O<sup>+•</sup>, the ionic product had an ion of m/z 96 (Figure 2c). Upon CID, the characteristic fragments of m/z 66 and m/z 65 were recorded (Figure 2d), with the loss of C<sup>18</sup>O (30 Da), [HC<sup>18</sup>O] • (31 Da), respectively. More convincingly, the fragment ions of m/z 66 themselves fragmented further to give ionic species of m/z 65, 51, 40, as recorded in the MS<sup>3</sup> spectrum (inset of Figure 2d), showing an identical fragmentation pattern observed for the major fragment (m/z66, Figure 2b) of  $C_6H_5^{16}OH^{+\bullet}$  (m/z 96). The exact m/zvalue measured with a high mass resolution for the ionic complex was 96.0456 (Supporting Information Figure S9b), matching the expected C<sub>6</sub>H<sub>5</sub><sup>18</sup>OH<sup>+•</sup> complex (theoretical value m/z 96.0456). When deuterated benzene was used, ions of m/z 99 (Supporting Information Figure S9c) were found, which generated daughter ions of m/z 71 (Supporting Information Figure S9d) at m/z99.0726 (Supporting Information Figure S9e), ideally matching the expected C<sub>6</sub>D<sub>5</sub>OH<sup>+</sup>• complex (theoretically valued at m/z 99.0727). These results suggested that the whole OH group of C<sub>6</sub>H<sub>5</sub>OH<sup>+•</sup> might be derived from the water radical cation. Traditionally, the synthesis of phenol requires harsh conditions through multi-step reactions, which brings less "green chemistry" and tedious treatment for by-products separation. In contrast, this work might lead to an alternative approach for phenol production with easy operation and maximal green chemistry.

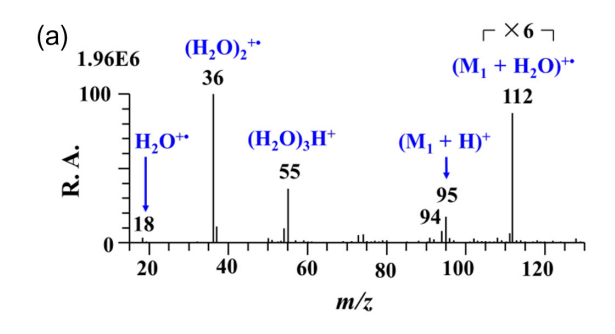
## Reaction between water radical cations and EA

Lipids are essential compounds in chemistry and biological objects in which water radical cations likely co-exist. Therefore, reactions between the water radical cation and EA (88 Da) were conducted, yielding the proton transfer

product (EA + H)<sup>+</sup> as well as a major product ion of m/z106 (Supporting Information Figure S13a). The exact mass for m/z 106 was 106.0624 (theoretical m/z 106.0624, Supporting Information Figure S14), suggesting the formation of a radical cation complex  $(EA + H_2O)^{+\bullet}$ . This was confirmed by CID (30% CE) of the mass-selected product ions (m/z 106), which generated a major peak at m/z 88 (Supporting Information Figure S13b) by the loss of H<sub>2</sub>O (18 Da). In Supporting Information Figure S13c, the abundance of ions of m/z 36  $(H_2O)_2^{+\bullet}$  decreased while that of ions of m/z 106 increased after the EA was introduced into the reaction. Therefore, it was proposed that  $(H_2O)_2^{+\bullet}$   $(m/z)_2^{+\bullet}$ 36) reacted with EA to produce a radical cation complex  $(EA + H<sub>2</sub>O)^{+\bullet}$  (m/z 106). However, no covalent bond cleavage in either EA or water was observed during the reaction or CID process of the  $(EA + H_2O)^{+\bullet}$ , suggesting that the EA was highly stable upon the attack of water radical cations, probably due to its unique molecular structure.

## Reaction between water radical cations and dimethyl disulfides

Disulfide bonds play key roles in biochemistry. To evaluate its vulnerability, the disulfide bond of dimethyl disulfide ( $CH_3SSCH_3$ ,  $M_1$ ), a mode of disulfide bond believed to be less active than those in typical biochemicals, reacted with  $(H_2O)_2^{+\bullet}$  (m/z 36) to generate the proton transfer product  $(M_1 + H)^+$  and disulfide-water radical complex  $(M_1 + H_2O)^{+\bullet}$  (m/z 112) (Figure 3a). The detection of the  $(M_1 + H_2O)^{+\bullet}$  complex was confirmed by the exact mass measurements (Supporting Information Figure S15a) with a mass accuracy of 0.9 ppm. In Supporting Information Figure S15b, we show that the signal of m/z 36 decreased dramatically after introducing dimethyl disulfide, indicating that the  $(H_2O)_2^{+\bullet}$   $(m/z)_2^{+\bullet}$ 36) reacted with dimethyl disulfide. Upon CID (30% CE), the ions of m/z 112 created predominant product ions of m/z 66 and m/z 65 in the MS/MS spectrum (Figure 3b), which were formed by the loss of CH<sub>2</sub>=S (46 Da) and CH<sub>3</sub>S<sup>•</sup> (47 Da), respectively, indicating that the disulfide



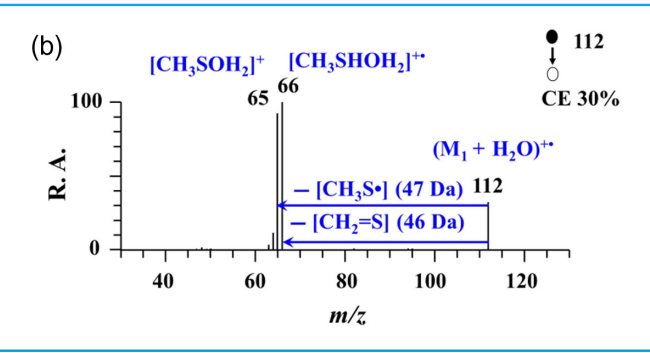


**Figure 3** | Mass spectrometric characterization of reaction between  $(H_2O)_2^{+\bullet}$  and dimethyl disulfide  $(M_1)$ . (a) Typical mass spectrum recorded with dimethyl disulfide showing  $[\mathbf{M_1} + H_2O]^{+\bullet}$  formation. (b) CID of  $[\mathbf{M_1} + H_2O]^{+\bullet}$ , m/z 112  $\rightarrow$  product ions.

**DOI:** 10.31635/ccschem.021.202101427

Corrected Citation: CCS Chem. **2022**, 4, 1224–1231 Previous Citation: CCS Chem. **2021**, 3, 3559–3566



bond in the complex (m/z 112) was activated upon binding to  $(H_2O)_2^{+\bullet}$ . Extra experimental data revealed two facts: (1) the nucleophilic and radical characteristics of  $(H_2O)_2^{+\bullet}$  both likely contribute to S-S cleavage and (2) the abundance ratio between the ionic fragments of m/z 66 and m/z 65 unity, due to the equal elimination of CH<sub>2</sub>=S (46 Da) and CH<sub>3</sub>S\* (47 Da) during the CID process. The fragment ions of m/z 66 and m/z 65, in turn, generated products of m/z 48 (Supporting Information Figure S16a) and m/z 47 (Supporting Information Figure S16b), both by the loss of  $H_2O$  (23% CE). Therefore, the precursor ions were ascribed to [CH3SH2OH2]\*\* and [CH<sub>3</sub>SOH<sub>2</sub>]<sup>+</sup>, respectively. Consequently, the overall results of the reactions between dimethyl disulfide and  $(H_2O)_2^{+\bullet}$  and the CID process are summarized in eq 2, as follows:

$$2H_3 + CSSCH_3 + 2(H_2O)_2^{+\bullet} \rightarrow [CH_3SOH_2]^+ + CH_3S + [CH_3SHOH_2]^{+\bullet} + CH_2 = S$$
 (2)

The reaction between  $(H_2O)_2^{+\bullet}$  and dimethyl disulfide was also confirmed by D2O isotope labeling experiments (Supporting Information Figures S17 and S18). In general, the experimental data demonstrated that the above reactions and the cleavage of disulfide bonds under the relatively mild conditions, indicating that the disulfide bonds in biomolecules might be attacked by water radical cations to cause an unexplored biochemical process.

#### Calculations and possible mechanism

The data gathered from the reactions did not only confirm the production of highly reactive water radical cations but also motivated us to probe the structural fundament of the reaction. Therefore, theoretical calculation of the  $(H_2O)_2^{+\bullet}$  structure was performed at the UCCSD(T)/ AUG-cc-pVTZ//UMP2/AUG-cc-pVDZ level. Our results demonstrated that there were two forms of water radical cations (Supporting Information Table S1) labeled as structure A and structure B. Structure A, containing the hydrogen atom bound, was of more stable structure and had bond lengths and angles consistent with a hydronium ion hydrogen-bonded to hydroxyl radical, with most of the charge on the hydronium ion.<sup>41</sup> The structure B was a true symmetrical dimer with a single-electron O-O bond (two electrons in a sigma bonding orbital and one in an antibonding orbital), in which the charge was equally shared by the two oxygen atoms. According to our calculations (Supporting Information Table S1), the bond between atom 2 (O) and atom 5 (H) in structure A was 1.469 Å, which was the longest, with the lowest bond energy. Theoretically, such a bond is easy to break, as observed in the CID experiments (Figure 2b). Similarly, the longest bond in structure B was located between the two oxygen atoms

(2.039 Å) and easiest to undergo cleavage, as shown in Figure 3b. Our calculations (Supporting Information Table S2) also showed that the fragmentation of both A and B isomers was endoergic. For instance, the proton-bound isomer (A) dissociated into H<sub>3</sub>O<sup>+</sup> and •OH by 94 kJ/mol and the O-O bonded isomer (B) dissociated into H<sub>2</sub>O<sup>+•</sup> and H<sub>2</sub>O by 165 kJ/mol (Supporting Information Table S3). Meanwhile, as shown in Supporting Information Table S1, the atom 2(0) in isomer A had the lowest charge (-0.346), therefore, could readily attack the benzene ring to form the intermediate, yielding the  $C_6H_5OH^{+\bullet}$ ,  $H_2$  and  $H_2O$  (detailed in Supporting Information Figures S19 and S20). Based on these results, benzene was oxidized mainly by isomer A, which provided the hydroxyl radicals, as confirmed by the data shown in Figure 2c (the isotope labeling experiment). The bond angle of H-O-H in isomer B was lower than in isomer A, probably because the lone pair in isomer B created a strong repulsion to hydrogen-oxygen bonds. Such a structure allowed the O-O group to simultaneously attack the disulfide bond in dimethyl disulfide (detailed in Supporting Information Figures S21 and S22), generating the characteristic fragments observed in CID experiments (Figure 3b). Therefore, the data suggest that the O-O single-electron bound dimer (B) mainly accounted for the unusual chemistry, such as the reaction with the disulfide bond of the water radical cations.

## **Conclusion**

Water radical cations  $(H_2O)_n^{+\bullet}$  (n = 2-5) were abundantly produced under ambient conditions using a homemade device based on energy-tunable discharge. The energy deposited on pure water vapor was changed by adjusting the experimental parameters such as discharge voltage (2.5 kV), the temperature of the MS inlet (140 °C), carrier gas flow (20 mL/min), and the distance between the discharge tip and the MS inlet. The results suggested that only suitable energy could produce abundant water radical cations. Due to the high reactivity of the as-prepared water radical cations, their formation was further confirmed by reacting with several substrates (benzene, EA, and dimethyl disulfide). Computations and experiments confirmed the existence of two forms of the dimer, a hydronium hydroxyl radical complex (A) and an O-O single-electron bound dimer (B), which accomplished interesting chemistry unexplored previously. This study has provided a convenient method for preparing adequate highly reactive water radical cations for advanced chemistry studies.

## **Supporting Information**

Supporting Information is available and includes experimental sections, Figures S1-S22, and Tables S1-S3.

**DOI:** 10.31635/ccschem.021.202101427

Corrected Citation: CCS Chem. 2022, 4, 1224-1231 Previous Citation: CCS Chem. 2021, 3, 3559-3566



### **Conflict of Interest**

There is no conflict of interest to report.

## **Acknowledgments**

This work was supported by a grant from the National Natural Science Foundation of China (grant no. 215201-02007) and the US National Science Foundation (grant no. 1905087).

#### References

- 1. Li, Z. B.; Loh, X. J. Water Soluble Polyhydroxyalkanoates: Future Materials for Therapeutic Applications. *Chem. Soc. Rev.* **2015**, *44*, 2865–2879.
- 2. Teixeira, E. S.; Uppulury, K.; Privett, A. J.; Stopera, C.; McLaurin, P. M.; Morales, J. A. Electron Nuclear Dynamics Simulations of Proton Cancer Therapy Reactions: Water Radiolysis and Proton- and Electron-Induced DNA Damage in Computational Prototypes. *Cancers* **2018**, *10*, 136.
- 3. Kearns, D. R.; Patel, D. J.; Shulman, R. G. High Resolution Nuclear Magnetic Resonace Studies of Hydrogen Bonded Protones of Transfer RNA in Water. *Nature* **1971**, 229, 338-339.
- 4. Pecourt, J. M. L.; Peon, J.; Kohler, B. Ultrafast Internal Conversion of Electronically Excited RNA and DNA Nucleosides in Water. *J. Am. Chem. Soc.* **2000**, *122*, 9348–9349.
- 5. Ball, P. Water as an Active Constituent in Cell Biology. *Chem. Rev.* **2008**, *108*, 74-108.
- 6. Kornblatt, J. A.; Kornblatt, M. J. Water as It Applies to the Function of Enzymes. *Int. Rev. Cytol.* **2002**, *215*, 49–73.
- 7. Pal, S. K.; Zewail, A. H. Dynamics of Water in Biological Recognition. *Chem. Rev.* **2004**, *104*, 2099–2124.
- 8. Ruotolo, B. T.; Giles, K.; Campuzano, I.; Sandercock, A. M.; Bateman, R. H.; Robinson, C. V. Evidence for Macromolecular Protein Rings in the Absence of Bulk Water. *Science* **2005**, *310*, 1658-1661.
- 9. Raschke, T. M. Water Structure and Interactions with Protein Surfaces. *Curr. Opin. Struct. Biol.* **2006**, *16*, 152–159. 10. Best, R. B.; Zheng, W. W.; Borgia, A.; Buholzer, K.; Borgia, M. B.; Hofmann, H.; Soranno, A.; Nettels, D.; Gast, K.; Grishaev, A.; Schuler, B. Comment on "Innovative Scattering Analysis Shows that Hydrophobic Disordered Proteins are Expanded in Water." *Science* **2018**, *361*, eaau8230.
- 11. Hincapié, G.; Acelas, N.; Castaño, M.; David, J.; Restrepo, A. Structural Studies of the Water Hexamer. *J. Phys. Chem.* **2010**, *114*, 7809-7814.
- 12. Garrett, B. C.; Dixon, D. A.; Camaioni, D. M.; Chipman, D. M.; Johnson, M. A.; Jonah, C. D.; Kimmel, G. A.; Miller, J. H.; Rescigno, T. N.; Rossky, P. J.; Xantheas, S. S.; Colson, S. D.; Laufer, A. H.; Ray, D.; Barbara, P. F.; Bartels, D. M.; Becker, K. H.; Bowen, H.; Bradforth, S. E.; Carmichael, I.; Coe, J. V.; Corrales, L. R.; Cowin, J. P.; Dupuis, M.; Eisenthal, K. B.; Franz, J. A.; Gutowski, M. S.; Jordan, K. D.; Kay, B. D.; LaVerne, J. A.; Lymar, S. V.; Madey, T. E.; McCurdy, C. W.; Meisel, D.; Mukamel, S.; Nilsson, A. R.; Orlando, T. M.; Petrik, N. G.; Pimblott, S. M.;

- Rustad, J. R.; Schenter, G. K.; Singer, S. J.; Tokmakoff, A.; Wang, L. S.; Wittig, C.; Zwier, T. S. Role of Water in Electron-Initiated Processes and Radical Chemistry: Issues and Scientific Advances. *Chem. Rev.* **2005**, *105*, 355–389.
- 13. Novakovskaya, Y. V.; Stepanov, N. F. Small Charged Water Clusters: Cations. *J. Phys. Chem. A* **1999**, *103*, 3285-3288.
- 14. Jiang, J. C.; Wang, Y.-S.; Chang, H.-C.; Lin, S. H.; Lee, Y. T.; Niedner-Schatteburg, G.; Chang, H. C. Infrared Spectra of H $^{\dagger}$ (H<sub>2</sub>O)<sub>5-8</sub> Clusters: Evidence for Symmetric Proton Hydration. *J. Am. Chem. Soc.* **2000**, *122*, 1398–1410.
- 15. Patten, R. A.; Gordy, W. Electron Spin Resonacne Investigations of Radication-Induced Free Radicals in DNA and RNA at Low Temperatures: Effects of Water. *Nature* **1964**, *201*, 361–363.
- 16. Ayotte, P.; Bailey, C. G.; Kim, J.; Johnson, M. A. Vibrational Predissociation Spectroscopy of the  $(H_2O)_6^{-\bullet}Ar_n$ ,  $n\geq 6$ , Clusters. *J. Chem. Phys.* **1998**, *108*, 444–449.
- 17. Jordan, K. D.; Johnson, M. A. Downsizing the Hydrated Electron's Lair. *Science* **2010**, *329*, 42-43.
- 18. Alizadeh, E.; Sanche, L. Precursors of Solvated Electrons in Radiobiological Physics and Chemistry. *Chem. Rev.* **2012**, *112*, 5578–5602.
- 19. Gardenier, G. H.; Johnson, M. A.; McCoy, A. B. Spectroscopic Study of the Ion-Radical H-Bond in  $H_4O_2^+$ . *J. Phys. Chem. A* **2009**, *113*, 4772-4779.
- 20. Mizuse, K.; Fujii, A. Characterization of a Solvent-Separated Ion-Radical Pair in Cationized Water Networks: Infrared Photodissociation and Ar-Attachment Experiments for Water Cluster Radical Cations  $(H_2O)_n^+$  (n = 3-8). *J. Phys. Chem. A* **2013**, *117*, 929–938.
- 21. Svoboda, O.; Hollas, D.; Ončák, M.; Slavíček, P. Reaction Selectivity in an Ionized Water Dimer: Nonadiabatic ab Initio Dynamics Simulations. *Phys. Chem. Chem. Phys.* **2013**, *15*, 11531–11542.
- 22. Wang, F.; Schmidhammer, U.; de La Lande, A.; Mostafavi, M. Ultra-Fast Charge Migration Competes with Proton Transfer in the Early Chemistry of H<sub>2</sub>O<sup>++</sup>. *Phys. Chem. Chem. Phys.* **2017**, *19*, 2894–2899.
- 23. Palmer, J. C.; Poole, P. H.; Sciortino, F.; Debenedetti, P. G. Advances in Computational Studies of the Liquid-Liquid Transition in Water and Water-Like Models. *Chem. Rev.* **2018**, *118*, 9129–9151.
- 24. de Visser, S. P.; de Koning, L. J.; Nibbering, N. M. M. Reactivity and Thermochemical Properties of the Water Dimer Radical Cation in the Gas Phase. *J. Phys. Chem.* **1995**, *99*, 15444–15447.
- 25. Shinohara, H.; Nishi, N.; Washida, N. Photoionization of Water Clusters at 11.83 eV: Observation of Unprotonated Cluster Ions  $(H_2O)^{n+}$  (2 $\le$ n $\le$ 10). *J. Chem. Phys.* **1986**, *84*, 5561–5567
- 26. Belau, L.; Wilson, K. R.; Leone, S. R.; Ahmed, M. Vacuum Ultraviolet (VUV) Photoionization of Small Water Clusters. *J. Phys. Chem.* **2007**, *111*, 10075–10083.
- 27. Yang, S.; Brereton, S. M.; Nandhra, S.; Ellis, A. M.; Shang, B.; Yuan, L. F.; Yang, J. Electron Impact Ionization of Water-Doped Superfluid Helium Nanodroplets: Observation of He (H<sub>2</sub>O)<sup>n+</sup> Clusters. *J. Chem. Phys.* **2007**, *127*, 134303.

**DOI:** 10.31635/ccschem.021.202101427 **Corrected Citation:** *CCS Chem.* **2022**, 4, 1224–1231 **Previous Citation:** *CCS Chem.* **2021**, 3, 3559–3566



- 28. Ma, J.; Wang, F.; Mostafavi, M. Ultrafast Chemistry of Water Radical Cation, H<sub>2</sub>O<sup>•+</sup>, in Aqueous Solutions. *Molecules* **2018**, *23*, 244.
- 29. Carroll, D. I.; Dzidic, I.; Stillwell, R. N.; Horning, E. C. Identification of Positive Reactant Ions Observed for Nitrogen Carrier Gas in Plasma Chromatograph Mobility Studies. *Anal. Chem.* **1975**, *47*, 1956–1959.
- 30. Dzidic, I.; Carroll, D. I.; Stillwell, R. N.; Horning, E. C. Comparison of Positive Ions Formed in Nickel-63 and Corona Discharge Ion Sources Using Nitrogen, Argon, Isobutane, Ammonia and Nitric Oxide as Reagents in Atmospheric Pressure Ionization Mass Spectrometry. *Anal. Chem.* **1976**, *48*, 1763-1768.
- 31. Kambara, H.; Mitsui, Y.; Kanomata, I. Identification of Clusters Produced in an Atmospheric Pressure Ionization Process by a Collisional Dissociation Method. *Anal. Chem.* **1979**, *51*, 1447–1452.
- 32. Kambara, H.; Kanomata, I. Determination of Impurities in Gases by Atmospheric Pressure Ionization Mass Spectrometry. *Anal. Chem.* **1977**, *49*, 270–275.
- 33. Radi, P. P.; Beaud, P.; Franzke, D.; Frey, H. M.; Gerber, T.; Mischler, B.; Tzannis A. P. Femtosecond Photoionization of (H<sub>2</sub>O)<sub>n</sub> and (D<sub>2</sub>O)<sub>n</sub> Clusters. *J. Chem. Phys.* **1999**, *111*, 512-518. 34. Mizuse, K.; Kuo, J. L.; Fujii, A. Structural Trends of Ionized Water Networks: Infrared Spectroscopy of

- Watercluster Radical Cations  $(H_2O)^{n+}$  (n=3-11). *Chem. Sci.* **2011**, *2*, 868–876.
- 35. Jonah, C. D. A Short Histroy of Radication-Chemistry of Water. *Radiat. Res.* **1995**, *144*, 141-147.
- 36. Dong, F.; Heinbuch, S.; Rocca, J. J.; Bernstein, E. R. Dynamics and Fragmentation of van der Waals Clusters:  $(H_2O)_n$ ,  $(CH_3OH)_n$ , and  $(NH_3)_n$  upon Ionization by a 26.5 eV Soft X-Ray Laser. *J. Chem. Phys.* **2006**, *124*, 224319.
- 37. Angel, L.; Stace, A. J. Dissociation Patterns of  $(H_2O)^{n+}$  Cluster lons, for n=2-6. *Chem. Phys. Lett.* **2001**, 345, 277-281.
- 38. Gaiduk, A. P.; Pham, T. A.; Govoni, M.; Paesani, F.; Galli, G. Electron Affinity of Liquid Water. *Nat. Commun.* **2018**, *9*, 247. 39. Tezuka, M.; Yajima, T.; Tsuchiya, A. Direct Hydroxylation of Aromatic Compounds in an RF Plasma. *Chem. Lett.* **1982**, *11*, 1437–1438.
- 40. Collyer, S. M.; McMahon, T. B. Proton Affinity of Water. A Scale of Gas-Phase Basicities including Ethylene and Water from Ion Cyclotron Resonance Proton Transfer Equilibrium Measurements. *J. Phys. Chem.* **1983**, *87*, 909-911
- 41. Cheng, Q.; Evangelista, F. A.; Simmonett, A. C.; Yamaguchi, Y.; Schaefer, H. F. Water Dimer Radical Cation: Structures, Vibrational Frequencies, and Energetics. *J. Phys. Chem. A* **2009**, *113*, 13779–13789.

DOI: 10.31635/ccschem.021.202101427 Corrected Citation: CCS Chem. 2022, 4, 1224-1231 Previous Citation: CCS Chem. 2021, 3, 3559-3566 Link to VoR: https://doi.org/10.31635/ccschem.021.202101427